Femtosecond time-resolved photoelectron-photoion coincidence imaging of multiphoton multichannel photodynamics in NO2

Vredenborg, A.; Roeterdink, W.; Janssen, M.H.M.

published in
Journal of Chemical Physics
2008

DOI (link to publisher)
10.1063/1.2924134

document version
Publisher's PDF, also known as Version of record

Femtosecond time-resolved photoelectron-photoion coincidence imaging of multiphoton multichannel photodynamics in NO_2

Arno Vredenborg, Willem G. Roeterdink, and Maurice H. M. Janssen[a)]
Laser Centre and Department of Chemistry, Vrije Universiteit, de Boelelaan 1083, 1081 HV Amsterdam, The Netherlands

(Received 27 March 2008; accepted 17 April 2008; published online 29 May 2008)

The multiphoton multichannel photodynamics of NO_2 has been studied using femtosecond time-resolved coincidence imaging. A novel photoelectron-photoion coincidence imaging machine was developed at the laboratory in Amsterdam employing velocity map imaging and "slow" charged particle extraction using additional electron and ion optics. The NO_2 photodynamics was studied using a two color pump-probe scheme with femtosecond pulses at 400 and 266 nm. The multiphoton excitation produces both NO_2^+ parent ions and NO^+ fragment ions. Here we mainly present the time dependent photoelectron images in coincidence with NO_2^+ or NO^+ and the (NO^+,e) photoelectron versus fragment ion kinetic energy correlations. The coincidence photoelectron spectra and the correlated energy distributions make it possible to assign the different dissociation pathways involved. Nonadiabatic dynamics between the ground state and the $A\ ^2B_2$ state after absorption of a 400 nm photon is reflected in the transient photoelectron spectrum of the NO_2^+ parent ion. Furthermore, Rydberg states are believed to be used as "stepping" states responsible for the rather narrow and well-separated photoelectron spectra in the NO_2^+ parent ion. Slow statistical and fast direct fragmentation of NO_2^+ after prompt photoelectron ejection is observed leading to formation of $NO^+ + O$. Fragmentation from both the ground state and the electronically excited $a\ ^3B_2$ and $b\ ^3A_2$ states of NO_2^+ is observed. At short pump probe delay times, the dominant multiphoton pathway for NO^+ formation is a 3×400 nm$+1\times266$ nm excitation. At long delay times (>500 fs) two multiphoton pathways are observed. The dominant pathway is a 1×400 nm$+2\times266$ nm photon excitation giving rise to very slow electrons and ions. A second pathway is a 3×400 nm photon absorption to NO_2 Rydberg states followed by dissociation toward neutral electronically and vibrationally excited $NO(A\ ^2\Sigma, v=1)$ fragments, ionized by one 266 nm photon absorption. As is shown in the present study, even though the pump-probe transients are rather featureless the photoelectron-photoion coincidence images show a complex time varying dynamics in NO_2. We present the potential of our novel coincidence imaging machine to unravel in unprecedented detail the various competing pathways in femtosecond time-resolved multichannel multiphoton dynamics of molecules. © *2008 American Institute of Physics*. [DOI: 10.1063/1.2924134]

I. INTRODUCTION

The invention of ion imaging[1] and velocity map imaging[2] has revolutionized our understanding of photodissociation dynamics. A wide body of literature is available now in which a dissociation process is initiated using nanosecond pulsed lasers and the products are detected using ion imaging.[3,4] The photoexcitation of NO_2 via the first excited state is known to be very complex due to a conical intersection coupling the ground and first excited states. The effect of this conical intersection has been extensively studied in the frequency[5,6] and more recently also the time domain.[7–10] Depending on the typical time scale of the dissociation dynamics, femtosecond pump-probe laser spectroscopy can be used. However, the high field strength of femtosecond pulses easily induce multiphoton transitions in molecules and in general different competing photon pathways will contribute to the observed dynamics. These competing pathways were reported in the first experiment combining femtosecond pump-probe spectroscopy and velocity map ion imaging on the multiphoton induced dynamics in CF_3I.[11] Even though ion imaging may provide more insight on the femtosecond dynamics, the electron produced in the ionization process contains a wealth of information on the photodynamics and goes by undetected in velocity map ion imaging experiments. Complementary to time-resolved imaging of ions, femtosecond photoelectron imaging was developed to study changes in the electronic character of evolving molecular states.[12] However, in the case of multiple ionic channels, the photoelectron spectra may get complex due to the contributions from electrons correlating with different ions. Therefore, the more powerful technique of photoelectron-photoion coincidence imaging[13] needs to be applied to obtain the full picture of the dynamics. By measuring the angular and energy distribution of the electron in coincidence with the angular and energy distribution of a mass selected ionic fragment, the most complete information about the bond breaking dynamics can be obtained in a single experiment.

[a)]Author to whom correspondence should be addressed. Electronic mail: mhmj@chem.vu.nl.

The Rydberg states of NO_2 and the photoionization dynamics of NO_2 have been studied using multicolor multiphoton laser radiation and single photon excitation with He I or synchrotron radiation.[14–19] The femtosecond time-resolved photoelectron-photoion coincidence imaging technique was pioneered by Hayden and co-workers and applied to NO_2,[20,21] CF_3I,[22] and the NO dimer.[23] In particular, Hayden and co-workers studied the femtosecond dynamics of NO_2 in a single color pump-probe experiment at 375 nm. At this wavelength, the dissociative multiphoton ionization dominates over the simple parent ionization, even though at 375 nm the first ionization potential of NO_2 is accessible by a three-photon absorption. The dominant dissociative multiphoton pathway was identified being a three photon excitation to a repulsive potential energy surface correlating to $NO(C\,^2\Pi)+O(^3P)$ followed by a one photon ionization to yield $NO^+(X\,^1\Sigma^+)+O(^3P)$. Singhal *et al.*[24] showed that with the same color laser light, 375.3 nm, but shorter pulses of about 50 fs, the NO^+ fragment was created via dissociation of NO_2 in the first excited state followed by three-photon ionization of the neutral $NO(X\,^2\Pi)$ fragment.

Two color femtosecond pump-probe spectroscopy in combination with fluorescence detection has been employed by López-Martens *et al.*[25] The NO_2 molecule was excited at 400 nm and the dissociation products were detected by dispersed fluorescence. The dominant dissociation pathway was initiated by three 3.1 eV (400 nm) photons, yielding $NO\,(A\,^2\Sigma^+)+O(^3P)$. It was found that $NO\,(A\,^2\Sigma^+)$ was predominantly produced in the vibrational ground and first excited state. Femtosecond fluorescence depletion spectroscopy yielded an upper limit for the dissociation time of 600 fs.

Eppink *et al.*[7] studied the dissociative multiphoton ionization of NO_2 by time-resolved velocity map imaging in a two-color pump probe experiment at 400 and 266 nm. The observed NO^+ signal was attributed to two competing mechanisms. The first mechanism involves a three-photon absorption at 400 nm followed by the dissociative ionization of the pumped state by a subsequent single 266 nm photon. The second mechanism involves a one-photon 400 nm absorption followed by a two 266 nm photon absorption giving rise to dissociative ionization of the parent molecule. In a follow-up study by this group, time-resolved velocity map ion imaging and photoelectron imaging was employed by Form *et al.*[8] In this experiment, the photoelectron and photoion were not detected in coincidence. Three significant photon pathways were observed contributing to the pump-probe transient of NO^+. No data were reported at negative delay times (corresponding to 266 nm pump) longer than the convolution time of the pump and probe laser. However, at small negative delay times, a contribution of the 266 nm photons acting as pump was observed for the formation of NO_2 ions and 1.5 eV photoelectrons. They ascribed this channel to a two 266 nm photon excitation to a 3*d* Rydberg state of NO_2 near 9.3 eV, after which the molecule absorbs one 400 nm probe photon for ionization. At small positive delay times (corresponding to 400 nm pump), a very short lived transient state was observed. The third pathway gives rise to a long lived pump-probe signal that exhibits a signature of wavepacket motion. The wavepacket motion has been attributed to the accidental energy match of the 3.1 eV pump photon with the lowest neutral dissociation channel $NO(^2\Pi)+O(^3P)$ near 3.18 eV. However, recent calculations[9,10] do not conclusively assign the mechanism of the variations in the NO^+ and electron transients.

Toffoli *et al.*[26] have recently reported the dissociative photoionization of NO_2 after single photon excitation by synchrotron radiation at 14.4 and 22.0 eV. They used coincidence imaging detection techniques and observed the recoil-frame photoelectron angular distribution for excitation at 14.4 eV to be anisotropic with the electron preferentially ejected in the plane of the molecule when the polarization is perpendicular to this plane.

In this paper, we present the first experimental results obtained with our newly constructed time-resolved photoelectron-photoion coincidence imaging machine in Amsterdam. In Sec. II we give a brief description of the new apparatus. In Sec. III we present coincidence data at various pump-probe delay times. From the correlation plots, we can assign the multiphoton dissociation pathways in NO_2 which are discussed in Sec. IV. In Sec. V, we summarize our main conclusions.

II. EXPERIMENTAL

A new time-resolved photoelectron-photoion coincidence imaging machine has been constructed in Amsterdam for the study of femtosecond photodynamics. In this section only a brief description of our experimental apparatus will be given, a full experimental paper with many details of the design and performance will be reported elsewhere.[27] The machine consists of three differentially pumped UHV chambers, the source chamber, a buffer chamber, and the imaging chamber. A continuous nozzle with a diameter of 100 μm is located in the source chamber. The supersonic molecular beam is skimmed by a 500 μm diameter skimmer (Beam Dynamics) positioned about 2 cm from the nozzle exit. The beam enters the differentially pumped second buffer chamber where a second 200 μm diameter skimmer, located 12 cm downstream from the first skimmer, separates the buffer chamber from the imaging chamber. In the imaging chamber, two time-of-flight (TOF) position- and time-sensitive particle detectors are mounted perpendicular to the molecular beam. The total distance between the nozzle and the laser interaction region is 45 cm.

With the molecular beam off the background pressure in the imaging chamber is better than 5×10^{-10} mbar. With the molecular beam on, and a backing pressure behind the nozzle of 1.0 bar, the pressure in the imaging chamber increases to about 2×10^{-9} mbar. We used a 1% mixture of NO_2 seeded in argon to prevent the formation of the NO_2 dimer.

To enable velocity map slice imaging of the charged particles, sets of open electrostatic lenses are positioned on both sides of the laser interaction region. After interaction of the NO_2 molecule with the pump and probe laser, the photoelectrons are extracted upwards into a 7 cm long TOF tube before hitting the electron detector. The typical flight time of the electrons is about 15 ns. Some 85 ns after the arrival of

the electron at the electron detector the electrostatic lenses are switched (with a 10%–90% rise time of about 45 ns) to set the proper voltages for velocity map imaging of the coincident ion. The ion is extracted into a 42 cm TOF tube before hitting the ion detector. Both the electron and the ion imaging detector consist of a chevron microchannel-plate stack in front of a delay line detector (Roentdek).

The mass resolution that we obtain from the full width half maximum of the arrival time of the various well-separated isotopes of Xe is $m/\Delta m \approx 4000$. The electron detector was calibrated in the energy range of 0–2 eV using multiphoton ionization of xenon and NO with femtosecond pulses at 400 and 266 nm. The energy bandwidth of our laser pulses for single photons are about 19 meV at 400 nm and 26 meV at 266 nm. The typical full width at half maximum (FWHM), kinetic energy resolution of the electron that we obtained for the present data is about 50 meV. Recent modifications in our setup have further improved our electron imaging and these improvements will be fully discussed elsewhere.[27]

The commercial laser system (Spectra Physics) consists of a titanium-sapphire oscillator (Mai-Tai) which, seeds the chirped regenerative amplifier (Spitfire Pro). The regen produces pulses with 500 μJ energy at a repetition rate of 5 kHz. A small percentage of the regen is split off and monitored online with a homebuilt autocorrelator. The shortest pulses obtainable from our regen are 130 fs. The typical length of the amplified pulses in the experiments reported here is set to about 160 fs to most efficiently double and triple the output pulses at 800 nm. The spectrum of the frequency doubled and tripled pulses is monitored with a spectrum analyzer (Ocean Optics). The typical pulse energies used are 15 μJ for the pump laser (400.4 nm) and 4 μJ for the probe laser (266.9 nm). The pump probe transients were recorded using slightly higher pulse energies of 20 μJ (400.4 nm) and 5 μJ (266.9 nm). A charge-coupled device (CCD) camera is used to measure the waist of the 400 nm pump beam at the distance corresponding to the position of the laser focus in the interaction region. The focus is measured to be about 100 μm in diameter.

III. RESULTS

A. Pump-probe transients

Two ions, the parent NO_2^+ and the fragment NO^+, are observed in the mass spectrum of the photoproducts of NO_2 after excitation with 400.4 and 266.9 nm photons. The pump-probe transients are shown in Fig. 1. A positive delay time indicates that the 400.4 nm laser is the pump pulse and the 266.9 nm laser the probe pulse. The inset in Fig. 1 gives the cross correlation width of about 244 fs by nonresonant ionization of xenon. The peak of the NO_2^+ transient is slightly shifted to negative time relative to the cross correlation peak of the xenon transient. From Fig. 1, it can be seen that the number of NO^+ fragment ions per laser shot is about a factor of 10 larger than the number of NO_2^+ parent ions. Only for the NO^+ fragment an enhancement is clearly observed at positive delay times, where the 400.4 nm photon is the pump and the 266.9 nm photon is the probe laser. In the pump-probe experiments of Eppink *et al.*[7] and Form *et al.*,[8] an oscillatory NO^+ transient was observed at positive delay time. Such a oscillatory pattern is not very distinctly observed in our present data although the small increases in our NO^+ transients at 1000 and 1500 fs are reproducible. The origin of the observed oscillations is still debated.[9,10] Our pump and probe pulses are about four times longer in duration compared to the pulses used by Eppink *et al.* and Form *et al.* Furthermore, a higher count rate per laser shot would probably improve the signal to noise ratio; however, the detection rate is somewhat limited due to our coincidence setup. These differences in the experimental conditions may explain the absence of a more pronounced oscillatory behavior in the NO^+ transient. In another femtosecond pump-probe setup in our laboratory in Amsterdam, using velocity map imaging of ions and electrons with a phosphor screen and CCD camera detector enabling multiple ions per laser shot, and a 1 kHz regen laser system with slightly shorter pulses, clear oscillations have been observed. A more focussed study on the oscillations will be presented elsewhere.[28]

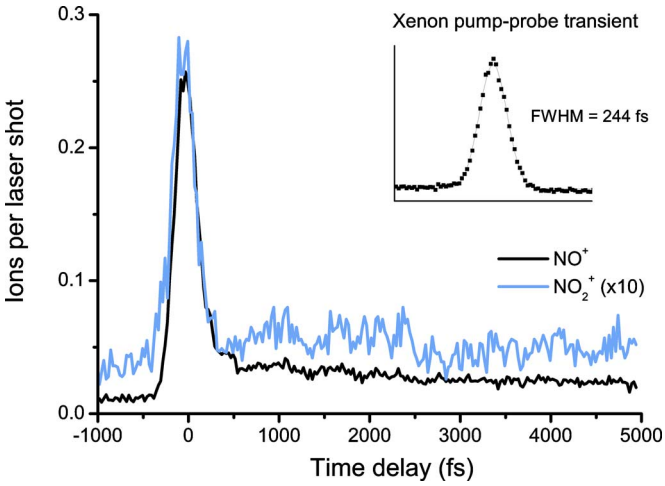

FIG. 1. (Color online) Pump probe transients for NO_2^+ and NO^+. A positive delay time means that the 266.9 nm probe pulse was crossing the molecular beam the indicated time after the crossing of the 400.4 nm pump pulse. The vertical axis displays the number of detected ions per laser shot. The pulse energies were about 20 μJ at 400.4 nm and 5 μJ at 266.9 nm, some 20%–30% higher than the pulse energies used for the coincidence measurements. The pump probe transient for the Xe ion, as measured under the same conditions, is included in the inset. The Xe ion is predominantly formed by a nonresonant multiphoton excitation with one photon at 400.4 nm and two photons at 266.9 nm. From the Xe transient, we obtain a FWHM cross-correlation width of about 244 fs.

B. Count and coincidence rates

The laser repetition rate of our experiment is 5 kHz. Our coincidence rate of 5% is a factor of 5 higher than in the experiments of Davies *et al.*[21] Too high count rates can give rise to false coincidences, i.e., the simultaneous detection of electrons and ions not originating from the same ionization event.[29] Figure 2 shows the time integrated electron images coincident with NO_2^+ and NO^+. From these images, it can be seen that the dominant feature in the NO electron image is arising from zero kinetic energy electrons, all focused in the middle of the image. However, the zero kinetic energy peak is completely absent in the electron image coincident with

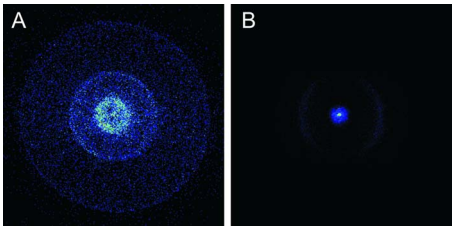

FIG. 2. (Color online) Time-integrated coincident electron images correlating with NO_2^+, panel A, and NO^+, panel B, taken at a pump probe delay time of 200 fs. The NO^+ electron image shows a dominant zero kinetic energy spot focussed in the center of the image.

NO_2^+. Moreover the femtosecond pump-probe excitation of NO_2 gives rise to dissociative ionization, in which predominantly NO^+ over NO_2^+ ions are formed. This complete absence of zero kinetic energy electrons in the NO_2^+ image is a strong indicator that false coincidences can be neglected even at the higher count rates that we have used. At each delay time coincidence events were collected during 1.8×10^7 laser shots, i.e., 1 h of measurement time. This means that a typical data file at long delay time contains some 5×10^5 (NO^+, e) coincidence events.

C. Coincident electron images

In the photoionization processes yielding the NO_2^+ parent ion, all the excess photon energy is carried away by the electron and as internal energy of the parent ion. The parent ion is created with no additional kinetic energy as it receives only a very small recoil kick from the ejected electron due to the conservation of linear momentum. Therefore, the velocity map imaging conditions make the parent ion appear only as a small spot in the center of the detector where the width along the molecular beam direction gives the translational energy distribution of the supersonic molecular beam. The mere fact that it is possible to focus the parent ions to a small point on the detector indicates the absence of N_2O_4 in the molecular beam, which would create NO_2^+ with kinetic energy from dissociation of the dimer.

The electron image coincident with the NO_2^+ parent ion at 200 fs delay of the 266.9 nm probe pulse relative to the 400.4 nm pump pulse is shown in Fig. 3(a) and is a 40° time slice of the three-dimensional electron distribution. The corresponding two-dimensional time-integrated position image was shown in Fig. 2(a). The kinetic energy distribution of the electrons is given in Fig. 3(b). Figure 3(c) shows the electron

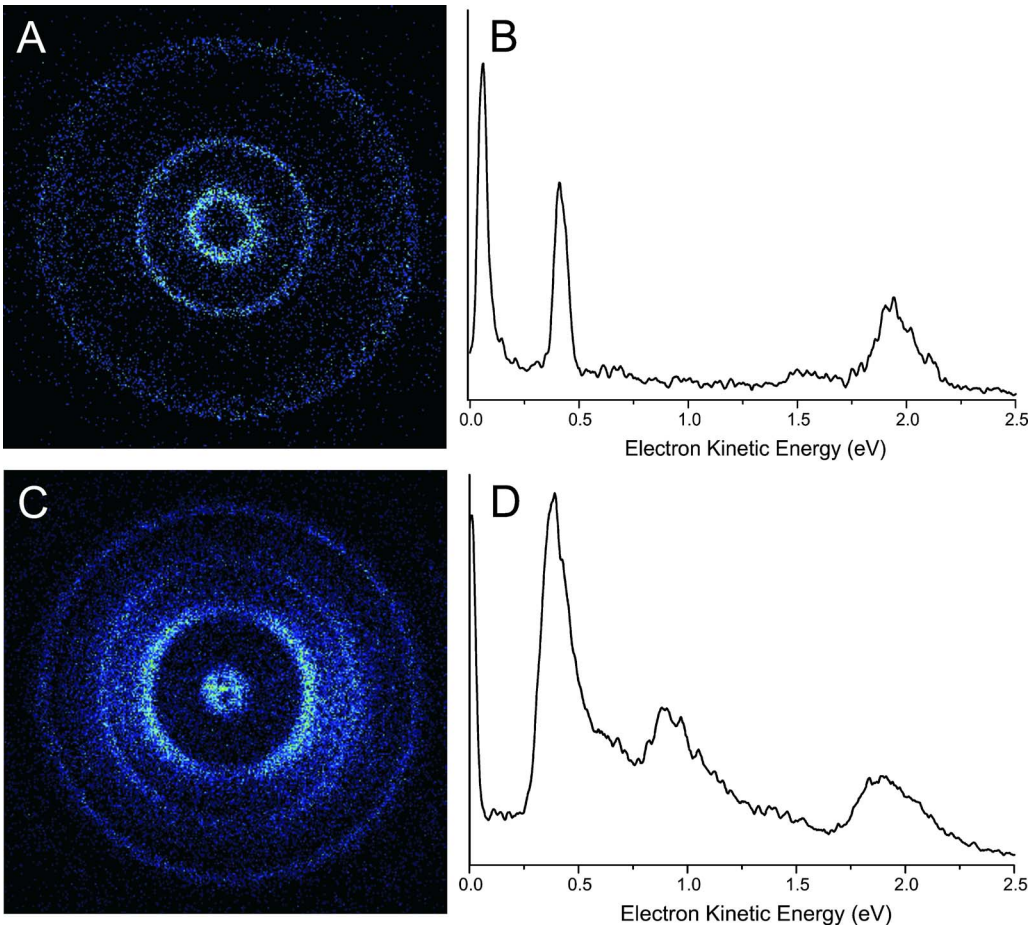

FIG. 3. (Color online) The electron slice images and the photoelectron energy distributions, coincident with NO_2^+ and NO^+ at a pump-probe delay time of 200 fs. The image represents a cut of those trajectories recoiling at an angle within ±20° with the plane defined by the direction of the polarization of the lasers, which is parallel to the direction of the molecular beam, and the propagation direction of the lasers. In panel A, an electron image and in panel B the distribution coincident with NO_2^+ is shown. In panel C, an electron image and in panel D the distribution coincident with NO^+ is shown. The vertical direction of the image is along the propagation direction of the laser. The distance from the center directly represents the observed velocity of the electrons. The radial integral of the electron image gives the kinetic energy. We show the photoelectron energy probability distribution.

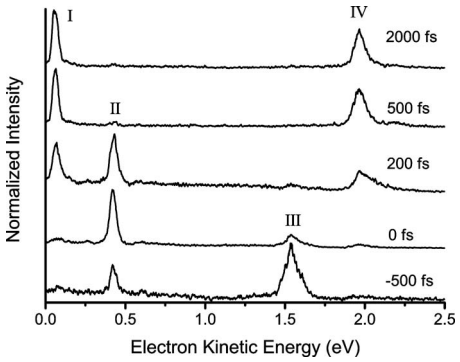

FIG. 4. Kinetic energy of the electrons coincident with NO_2^+ as a function of pump probe delay time. The different peaks are labeled (I)–(IV) and are discussed in the text. The photoelectron traces at each delay time are normalized. To compare the spectra at different delay times, the following number of total electrons in coincidence with NO_2^+ can be used (in kiloevents), 59 (−500 fs), 116 (0 fs), 71 (200 fs), 75 (500 fs), and 75 (2000 fs).

image correlating with the NO^+ fragment at the same delay time of 200 fs and is a 40° time slice of the three-dimensional electron distribution. The corresponding two-dimensional time-integrated position image was shown in Fig. 2(b). The kinetic energy distribution of the electrons is shown in Fig. 3(d).

We have measured coincidence data at various pump-probe delay times. In Fig. 4, we show the kinetic energy distribution of the electrons coincident with the NO_2^+ parent ion and in Fig. 5 for the NO^+ ion at the indicated pump-probe delay time. The electron peaks in coincidence with NO_2^+ are labeled (I)–(IV) in Fig. 4 and the electron peaks in coincidence with NO^+ are labeled (1)–(7) in Fig. 5.

To help the interpretation of the various multiphoton pathways responsible for the various peaks, we have also taken coincidence data with the 400 nm pulse only. The resulting coincidence photoelectron spectrum for NO_2^+ is shown in Fig. 6. In this case, a similar laser pulse energy of about 15 μJ was used. We will discuss the origin of the various peaks in Sec. IV.

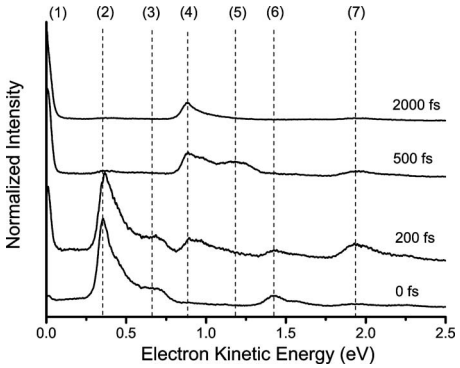

FIG. 5. Kinetic energy of the electrons coincident with NO^+ as a function of pump probe delay time. The different peaks are labeled (1)–(7) and correspond with the labeled regions in the energy correlation plots, see Fig. 7. The photoelectron traces at each delay time are normalized. To compare the spectra at different delay time the following number of total electrons in coincidence with NO^+ can be used (in kiloevents), 600 (0 fs), 420 (200 fs), 408 (500 fs), 284 (2000 fs).

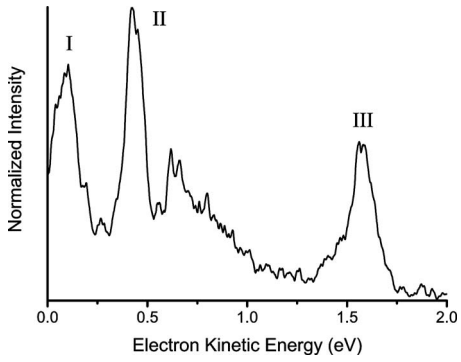

FIG. 6. Kinetic energy of the electrons coincident with NO_2^+ for excitation with 400 nm pulses only. The labels (I), (II), and (III) correspond to the similar electron peaks observed in the two laser pump-probe experiment, see Fig. 4.

D. Photoion-photoelectron energy correlation

Conservation of energy imposes an important constraint on the origin of the observed electron peaks. We can express this constraint as follows:

$$E_{\text{photon}} - AE = E_{\text{kin,tot}} + E_{\text{int}} + E_{\text{electron}}, \tag{1}$$

where E_{photon} is the total excitation energy of the molecule, AE is the appearance energy of the fragments, $E_{\text{kin,tot}}$ is the total kinetic energy of the fragments, E_{int} is the internal energy of the produced fragments, and E_{electron} is the kinetic energy of the coincident electron. The appearance energy of the energetically lowest accessible channel producing NO^+ is[18,26]

$$NO_2 \rightarrow NO^+(^1\Sigma) + O(^3P) + e^-, \quad AE = 12.38 \text{ eV}. \tag{2}$$

As only two fragments are formed and because of the conservation of momentum the total kinetic energy of the fragments can be expressed as a function of the kinetic energy of the NO^+ fragment,

$$E_{\text{kin,tot}} = E_{\text{kin,NO}}\left(1 + \frac{m_{\text{NO}}}{m_{\text{O}}}\right). \tag{3}$$

In Fig. 7, we present the energy correlation plots for the NO^+ fragment at three different pump-probe delay times. The vertical axis of the correlation plots shows the kinetic energy of the electron and the horizontal axis the total kinetic energy of all fragments. The diagonal lines indicate upper bounds for the energy for a specific multiphoton process. The various labels (1)–(7) correspond to the same peaks as in Fig. 5.

E. Recoil-frame photoelectron angular distribution

In Fig. 8(a), we show the recoil-frame photoelectron angular distribution (RFPAD), at zero delay time, for correlated (NO^+, e) events where the NO^+ ion is recoiling with a kinetic energy of 0.3 ± 0.1 eV and the photoelectron ejected with an energy of 0.65 ± 0.06 eV. Only those events were selected where the NO^+ fragment was recoiling within 15° of the direction of the (parallel) polarization of the pump and probe lasers. In Fig. 8(b), we show the RFPAD for (NO^+, e) events where the NO^+ ion is recoiling with a kinetic energy of about 1.0 ± 0.1 eV and the photoelectron with an energy of

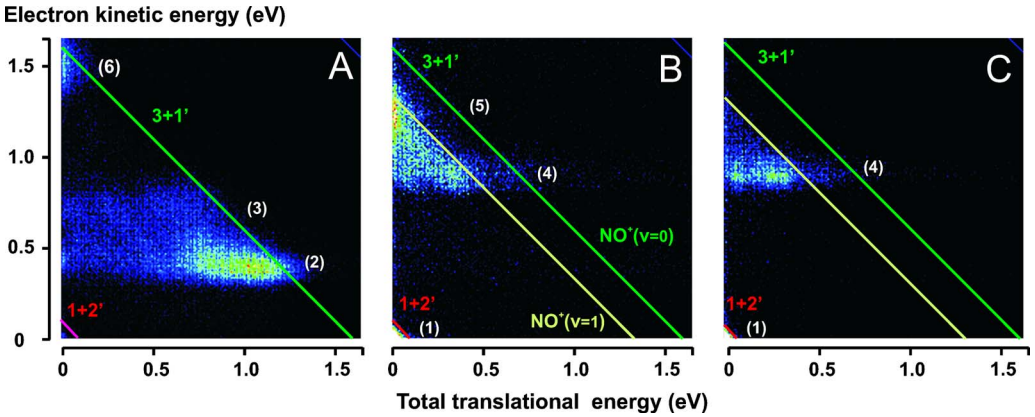

FIG. 7. (Color online) Energy correlation plots of the (NO^+,e) events at three different delay times, 0 fs (A), 500 fs (B), and 1750 fs (C). The diagonal dark green line, labeled with $3+1'$, near 1.55 eV gives the total available energy for electron and fragments for excitation with three photons at 400.4 nm plus one photon at 266.9 nm, a $(3+1')$ process. The red diagonal line, labeled with $(1+2')$, at 60 meV gives the upper boundary of the available energy for excitation with one photon at 400.4 nm plus two photons at 266.9 nm, a $(1+2')$ process. A diagonal line at 1.3 eV shows the upper boundary of the available energy for the channel leading to vibrationally excited $NO^+(v=1)$ after excitation with three photons at 400.4 nm plus one photon at 266.9 nm.

0.35 ± 0.03 eV. Finally, in Fig. 8(c), we show the RFPAD at 2000 fs delay time for (NO^+,e) events where the NO^+ ion is recoiling with a kinetic energy of 0.3 ± 0.1 eV and the photoelectron with an energy of 0.93 ± 0.05 eV. As can be seen in Figs. 8(a) and 8(b) a strong but differing asymmetry is observed in the RFPAD with a preferential ejection of the photoelectron in the direction of the NO^+ direction. In Fig. 8(c), a symmetrical forward-backward RFPAD is observed. These representative RFPADs and their underlying multiphoton mechanism will be briefly discussed in Sec. IV.

IV. DISCUSSION

In Fig. 9, we present a schematic energy diagram of the various electronic levels in NO_2 and the neutral and ionic fragmentation channels. We labeled the various processes with the same labels (I)–(IV) and (1)–(7) as in Figs. 4, 5, and 7. In Table I, we list the adiabatic and vertical ionization energies of various excited states of the NO_2^+ ion of relevance here and reported before in the literature.[16–18,30] In Table II, we list the total photon excitation energy for various combinations of multiphoton excitation with 400.4 and 266.9 nm photons. Because the pump and probe pulses are harmonics of the 800.8 nm fundamental output of the regen laser it is to be noted that two photons at 266.9 nm represent the same amount of energy as three photons at 400.4 nm. In the following discussion, we will label the number of 266.9 nm photons with a prime, e.g., a notation $(1+2')$ means a multiphoton process involving one photon at 400.4 nm and two photons at 266.9 nm.

A. Multiphoton pathways for formation of $NO_2^+ + e$

In the formation of the parent ion, all the excess energy is funneled into kinetic energy of the electron and internal excitation of the NO_2^+ parent ion. In the photoelectron spectrum of Fig. 4, we observe two rather narrow peaks near 60 meV (I) and 400 meV (II) and two somewhat wider bands near 1.55 eV (III) and 1.9 eV (IV).

The adiabatic ionization energy of NO_2 is 9.586 eV.[16,31,32] Because of the large change in geometry between the bent ground state of the neutral molecule and the linear ground state of the ion one-photon ionization results in a spectrum to higher energy than the adiabatic ionic ground state. Baltzer *et al.*[17] observed the onset of the ionic ground state near 10.3 eV and the center of the band near 11.2 eV, substantially higher than the adiabatic energy of 9.586 eV.[31,32] Grant and co-workers[14–16] have used multicolor double-resonant multiphoton excitation with tunable nanosecond lasers to study Rydberg states in NO_2 and the state-selective production of vibrationally excited NO_2^+. This double-resonant scheme makes it possible to prepare low lying vibronic states in the $3p\sigma$ and $3p\pi$ Rydberg states of NO_2. They identified the vibrationless (000) origin of the $3p\sigma\ ^2\Sigma_u^+$ state at 55 649 cm^{-1} (6.9 eV) and the $3p\pi\ ^2\Pi_u$ state at 57 990 cm^{-1} (7.19 eV).

The lowest possible multiphoton excitation producing the parent ion is a two 400.4 nm photon plus one 266.9 nm photon excitation, i.e., a $(2+1')$ excitation. This results in a total photon excitation energy (see Table II) of 10.84 eV, in the region of the ground state $X\ ^1\Sigma_g^+$ and below the first electronically excited (bent) $a\ ^3B_2$ (000) state of the NO_2^+ ion, see Table I. If such a $(2+1')$ process would happen and produce a NO_2^+ ion in the vibrational ground state, an electron peak at maximum energy of $10.84-9.586=1.25$ eV should be formed. In the various time-dependent photoelectron spectra of Fig. 4, we do not see any peak at 1.25 eV. The peaks (III) and (IV) are formed at higher energy and therefore must be produced by a different multiphoton process at higher total excitation energy.

The peaks (I) and (II) are in principle energetically possible to result from a $(2+1')$ excitation process; however, we think this is not the case because of the following reasons. In Fig. 6, we show the photoelectron spectrum from an experiment using excitation by the 400.4 nm pulse only, and we identified the electron peaks at similar energy as in Fig. 4 with the same labels (I),(II), and (III). We see a somewhat broader peak at low energy of about 100 meV, peak (I), and a somewhat narrower peak near 400 meV, peak (II). The lowest number of 400.4 nm photons that can produce these photoelectrons is 4, i.e., $(4+0')$. This results in a total exci-

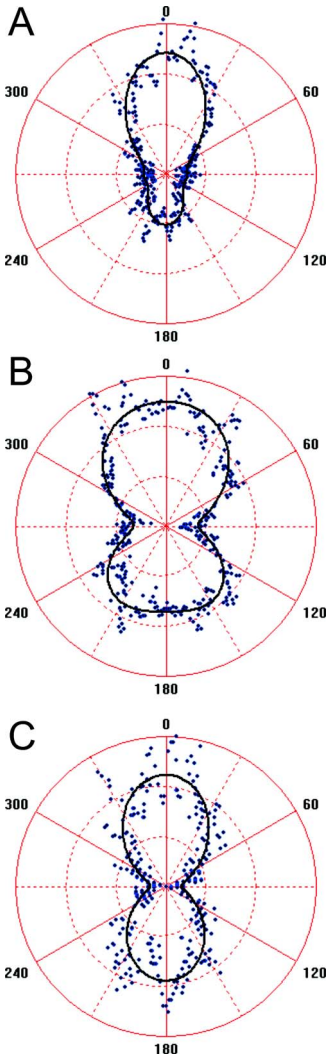

FIG. 8. (Color online) RFPAD. The angular distribution of the ejected electron with respect to the NO^+ direction is plotted for selected regions of photoelectron energy and correlated fragment kinetic energy at specific pump-probe delay time. Only (NO^+,e) events are selected where the ion is ejected with a polar angle less than 15° with the direction of the (parallel) polarizations of pump and probe laser beams. The selected events were as follows: Panel A: delay time is 0 fs; photoelectron energy 0.65 ± 0.06 eV; fragment total kinetic energy 0.3 ± 0.1 eV. Panel B: delay time is 0 fs; photoelectron energy 0.35 ± 0.03 eV; fragment total kinetic energy 1.0 ± 0.1 eV. Panel C: delay time is 2000 fs; photoelectron energy 0.93 ± 0.05 eV; fragment total kinetic energy 0.3 ± 0.1 eV. The processes in panels A and B are attributed to a $(3+1')$ excitation with fragmentation on the $a\ ^3B_2$, $b\ ^3A_2$ electronically excited states of the NO_2^+ ion. The process in panel C is attributed to a $(3+1')$ excitation leading to neutral NO $(A\ ^2\Sigma v=1)+O$, followed by single photon ionization of NO.

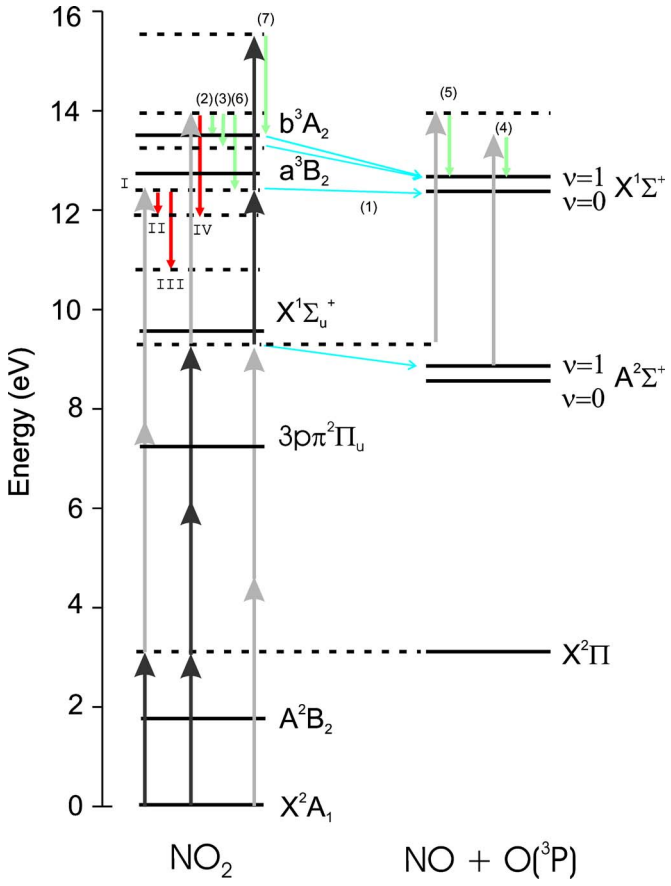

FIG. 9. (Color online) Energy levels of NO_2 and the various photofragmentation and ionization channels. Indicated are the assigned multiphoton pathways which are discussed in the text. A 266.9 nm photon is represented by a light gray arrow and the 400.4 nm by a dark gray arrow. The red arrows (labeled with II, III, IV) correspond to electrons observed in coincidence with NO_2^+, while the green arrows [labeled with (2), (3), (4), (5), (6), (7)] correspond to electrons detected in coincidence with NO^+. No colored electron arrows are drawn for the very slow electrons corresponding to peaks I and (1). The blue lines indicate dissociation dynamics in the neutral NO_2 molecule or the NO_2^+ ion.

tation energy of 12.4 eV, below the first electronically excited state of the NO_2^+ ion, see Table I. Because these photoelectron energies are similar to the energies of peaks (I) and (II), we conclude that peaks (I) and (II) result from a process equal in energy to an integer number of 400.4 nm photons, for instance, equal in energy to a $(4+0')$ process. Returning to the peaks observed in the pump-probe experiment, a $(2+1')$ process is equal in excitation energy to 3.5 photons of 400.4 nm and this is not an integer number of 400.4 nm photons. Furthermore, peak (I) is a photoelectron produced from a long lived NO_2 neutral state formed after excitation by the 400.4 nm pump pulse. At two-photon excitation of 400.4 nm, the total energy is 6.2 eV. At this energy, there is no long lived bound state in NO_2.[33] Therefore, we conclude that peaks (I) and (II) cannot result from the lowest energy excitation pathway of $(2+1')$ but must result from a different multiphoton excitation.

TABLE I. Ionization energies (Refs. 16, 17, 19, and 30) and lifetimes (Ref. 18) of ionic states in NO_2.

Electronic state	Adiabatic energy (eV)	Vertical energy (eV)	lifetime (μs)	NO^+ branching (%)
$X\ ^1\Sigma_g^+$	9.586	11.2	Stable	0
$a\ ^3B_2$ (000)	12.767[a] 12.862[b]	13.06	>150	0
$a\ ^3B_2$ (100)	12.93[c]	⋯	20	3%
$a\ ^3B_2$ (200)	13.10[c]	⋯	3.5	20%
$a\ ^3B_2$ (300)	13.27[c]	⋯	0.3	72%
$b\ ^3A_2$ (000)	13.592[a] 13.593[b]	13.69	10^{-5}	100
$A\ ^1A_2$ (000)	14.066	14.13	0.8	100

[a]Reference 17.
[b]Reference 19.
[c]Assuming a vibrational ν_1 modes energy of 170 meV, similar to the energy of the ν_1 in the $X\ ^1\Sigma_g^+$ ground state (175 meV) and the $b\ ^3A_2$ state (169 meV) (Ref. 17).

TABLE II. Total photon excitation energy for various combinations of pump and probe photons. The FWHM of the energy width of a single photon due to the short duration of the laser pulse is about 19 meV at 400.4 nm and 26 meV at 266.9 nm.

No. of 400.4 nm photons	No. of 266.9 nm photons	Total excitation energy (eV)
1	0	3.096
0	1	4.645
1	1	7.73
3	0	9.29
0	2	9.29
2	1	10.84
4	0	12.39
1	2	12.39
3	1	13.93
2	2	15.48

The multiphoton excitation which is next to lowest in total energy is a $(1+2')$ process at 12.4 eV and this is equal in energy to four photons of 400.4 nm, see Table II. Such an $(1+2')$ excitation starts by first the absorption of one photon of 400.4 nm which is just below the dissociation threshold of NO_2 and at the maximum of the absorption band formed by the vibronically strongly coupled $X\ ^2A_1$ and $A\ ^2B_2$ electronic states.[9,34] Peak (I) is not visible at time overlap, contrary to peak (II). Furthermore, peak (II) disappears on the same time scale of about 100–200 fs as that peak (I) appears. This seems to suggest that some dynamics is needed to evolve after absorption of the 400.4 nm photon that simultaneously results in the appearance of photoelectron peak (I), being probed by two-photon ionization, and the disappearance of photoelectron peak (II). Furthermore, the width of both photoelectron peaks is rather narrow suggesting that the ionization probes geometries of the NO_2 neutral molecule which are very similar to the linear geometry of the ion.

As stated earlier absorption near 400.4 nm results in excited NO_2 in a region of strongly coupled states $X, A\ ^2B_2$.[9,34] The recent quantum mechanical wavepacket calculations of the nonadiabatic dynamics in NO_2 by Sanrey *et al.*[9] show that for a wavepacket starting on the excited electronic state the population decays in some 200 fs to about 0.5 of the initial population and stays rather constant for time scales calculated up to 500 fs, see Fig. 4 in Ref. 9. This time scale of 100–200 fs corresponds well with the similar time scale that we see for the appearance and disappearance of peaks (I) and (II) in Fig. 4. The fact that we see peak (II) at higher photoelectron disappears is in agreement with a mechanism of population loss and spreading of the wavepacket on the excited state. Subsequent ionization of the wavepacket on the excited state by two photons of 266.7 nm to give photoelectron peak (II) is reduced and completely hampered after some 200 fs.

The total energy of $(1+1')$ excitation, i.e., one photon of 400.4 nm and one photon of 266.7 nm, results in an excitation energy of 7.74 eV. This is exactly in the region of vibrationally excited levels of the $3p\pi\ ^2\Pi_u$ Rydberg state.[14,15] Further absorption of a second 266.7 nm photon from this Rydberg state will produce NO_2^+ ions in coincidence with electrons with a rather narrow kinetic energy distribution due to the similarity of the Rydberg state with the ground state of the NO_2^+ ion. This width may be mainly determined by the total energy spread of the multiphoton excitation due to the short femtosecond pulses. The energy difference of 360 meV between peaks (I) and (II) is close to the energy of two quanta of symmetric stretch, ν_1, vibration in the $3p\pi\ ^2\Pi_u$ Rydberg state, or a combination mode of one quantum of symmetric stretch and two quanta of bending, ν_2.[14–16]

The laboratory frame photoelectron angular distribution of peaks (I) and (II) appear to be very isotropic. We can expand the laboratory frame angular distribution of electrons in Legendre polynomials, $I_{\mathrm{lab},e}=1+\Sigma\beta_{i,\mathrm{lab},e}P_i$, with $i=2,4$. For peak (I), we find $\beta_{2,lab,e}(\mathrm{I})\approx -0.1$ and $\beta_{2,lab,e}(\mathrm{II})\approx 0.3$. These small values reflect the ejection of (predominant) isotropic *s* partial waves. This is in agreement with the expected laboratory frame electron angular distribution resulting from a one-photon ionization of a Rydberg state of $3p\pi\ ^2\Pi_u$ character.

We will now discuss the origin of peaks (III) and (IV) at higher photoelectron energies of 1.55 and 1.9 eV, respectively. Peak (III) is only observed at delay time near zero and at negative times, i.e., when the 266.9 nm pulse is the pump beam. This suggests that peak (III) results from an excitation with 266.9 nm photons first followed by the absorption of one or more photons of 400.4 nm. Comparison to the photoelectrons observed in the experiment with 400.4 nm photons only, we see in the top panel of Fig. 6 a peak around 1.5 eV as well, suggesting that the total excitation energy of peak (III) is equal to an integer number of 400.4 nm photons. The lowest multiphoton process, equivalent to an integer number of 400.4 nm photons, and allowing the ejecting of an electron of 1.4 eV would be a $(2'+1)$ process, i.e., a two-photon excitation at 266.9 nm followed by the absorption of a single photon of 400.4 nm. The two-photon excitation at 266.9 nm gives a total energy of 9.29 eV. This is in the region of several higher lying Rydberg states of NO_2. Petsalakis *et al.*[35] assigned the $3d\ 5^2A_1$ Rydberg state at a vertical transition energy of 9.28 eV above the ground state. Furthermore, we observe a much more anisotropic laboratory frame angular distribution of photoelectrons at peak (III); we find $\beta_{2,\mathrm{lab},e}(\mathrm{III})\approx 1.3$. At time zero we even find a small positive contribution of a fourth order Legendre polynomial, $\beta_{4,\mathrm{lab},e}(\mathrm{III})\approx 0.3$. This would be in agreement with the expected much more anisotropic photoelectron distribution resulting from the partial waves of *p* and *f* symmetries after one-photon ionization of a *3d* Rydberg electron. This peak near 1.5 eV was also observed by Form *et al.*[8] and attributed to the same $(2'+1)$ process, even though their signal to noise ratio was not sufficient enough to extract the angular distribution. Our results appear to support the assignment of peak (III) to this multiphoton process. However, at this point we would like to remark that the theoretical calculations of the vertical energies of the high Rydberg states appear not to be of high enough accuracy.[35] The adiabatic and vertical ionization energies of NO_2 are calculated at energies of 8.83 and 10.42 eV, i.e., about 0.76–0.78 eV lower than the experimental values.

The electron peak (IV) near 1.9 eV is not present yet

near zero delay time and is not observed in the experiment with 400.4 nm only. This suggests again that some dynamics is needed to produce this peak and that an excitation energy equal to a noninteger number of 400.4 nm photons is involved. We assign peak (IV) to a $(3+1')$ process at a total energy of 13.93 eV. A prompt photoelectron of 1.9 eV will leave the NO_2^+ ion at an energy of about 12 eV well below the adiabatic energy of the first excited $a\ ^3B_2$ (000) ionic state. The energy of three photons of 400.4 nm is equal to 9.29 eV; this is in the region of highly excited Rydberg states in NO_2. Perhaps within the relatively long pulse duration of our 400.4 nm pump pulse, a similar nonadiabatic dynamics occurs first after absorption of one photon of 400.4 nm. Then within the 150 fs pulse duration of the 400.4 nm further excitation with two photons of 400.4 nm occurs to a long lived Rydberg state. This state is then probed by the delayed 266.9 nm probe laser resulting in the ejection of a photoelectron of 1.9 eV. The anisotropy of the angular distribution of photoelectrons of peak (IV) is $\beta_{2,\mathrm{lab},e}(\mathrm{IV}) \approx 0.5-0.7$.

B. Multiphoton pathways for formation of $NO^+ + O + e$

In Figs. 5 and 7, we have numbered the various photoelectron peaks and the (e, NO^+) energy correlation regions (1)–(7). We will now discuss the multiphoton pathways and distinguish two regions, short pump-probe time delay up to about 200 fs, within the cross correlation time resolution of the pump-probe pulses, and long pump-probe delay from about 200 to 2000 fs.

1. Short time delay

The peaks numbered (2), (3), and (6) at electron energies of about 0.35, 0.65, and 1.4 eV are observed at short delay times of 0–200 fs and are absent at time delays of 500 fs or longer. The similar time dependence suggests they originate from a similar multiphoton pathway. Using the experimental value of the NO_2 dissociation threshold $D_0 = 25\,128.57\ \mathrm{cm}^{-1}$ (Ref. 36) and the ionization energy of NO, IE=9.2642 eV,[37] the thermodynamic threshold for the formation of $NO^+(^1\Sigma) + O(^3P) + e$ can be calculated to be 12.38 eV. This threshold is very close to the excitation with one photon at 400.4 nm and two photons of 266.9 nm (see Table II), a $(1+2')$ excitation at 12.39 eV leaving almost no energy for the electron or kinetic energy of the fragments. This pathway will be discussed below in Part 2 discussing the long delay time dynamics.

The next multiphoton pathway is a $(3+1')$ excitation with a total excitation energy of 13.93 eV, well above the thermodynamic threshold for the formation of $NO^+(^1\Sigma)$. As can be seen in the energy correlation plot of Fig. 7(a), the total kinetic energy of the electron peaks (2), (3), and (6) and the correlated fragments $NO^+(^1\Sigma) + O(^3P)$ are bounded by the energy for an excitation with three photons at 400.4 nm and one photon at 266.9 nm indicated by the green line at an energy of 13.93–12.38=1.55 eV.

Peak (6), producing very fast electrons at 1.4 eV and very slow $NO^+(^1\Sigma)$, suggests a slow statistical dissociation of NO_2^+ after prompt ejection of a fast electron. It leaves the NO_2^+ parent system at an energy just above the thermodynamic threshold for the formation of $NO^+(^1\Sigma) + O(^3P)$. The excitation pathway $(3+1')$ apparently accesses configurations of the NO_2 neutral molecule that can slowly dissociate on the ionic NO_2^+ ground state surface at an energy just above the thermodynamic threshold.

Peaks (2) and (3), with electron kinetic energies near 0.35 and 0.65 eV, are only observed within the cross correlation width and are bounded by the $(3+1')$ available energy. The structure of the energy correlation in Fig. 7(a) is horizontal and does not resemble the more diagonal structures observed in the (NO^+, e) correlation plots by Davies *et al.*[20] in the pump-probe coincidence imaging experiment with one color four-photon excitation at 375.3 nm at zero time delay. This latter pathway was identified to be an excitation at the three-photon level to a dissociative neutral NO_2 state that dissociates to the neutral $NO(C\ ^2\Pi) + O(^3P)$ channel. During the 100 fs pulse duration the bond stretches and the system can absorb a fourth-photon over a relative large configuration space leading to an inverse correlation between the electron energy and the fragments kinetic energy.

The horizontal structures (2) and (3) in our energy correlation plot, Fig. 7(a), suggest a prompt electron ejection. Region (2) produces rather fast fragments with a total kinetic energy peaking around 1.1 eV. This suggests a prompt and fast dissociation. If we subtract the electron energy of about 0.35 eV of region (2) from the total excitation energy of 13.93 eV, we obtain an energy of 13.58 eV. This is exactly at the observed adiabatic energy of 13.59 eV of the $b\ ^3A_2$ (000) electronically excited state of the NO_2^+ parent. This state was studied by Baltzer *et al.*[17,18] and observed to have a very short lifetime of about 100 fs and to completely dissociate to $NO^+ + O$. The laboratory frame angular distributions of these electrons correlating with NO^+ are $\beta_{2,\mathrm{lab},e}(2) = 0.8$ and $\beta_{4,\mathrm{lab},e}(2) = -0.3$. This is a very similar $\beta_{2,\mathrm{lab},e}(2)$ as the $\beta_{2,\mathrm{lab},e}(\mathrm{IV}) \sim 0.5-0.7$ observed for peak (IV) correlating with and attributed to the same $(3+1')$ process, see Sec. IV A.

The second region labeled (3) shows a somewhat broader range of kinetic energy of fragments and photoelectrons peaking around 0.65 eV with a cutoff near 0.8 eV. If we subtract the photoelectron energy of 0.65 eV from the total excitation energy of 13.93 eV, we obtain an energy of 13.28 eV. This is near the estimated adiabatic energy of 13.27 eV of the (300) level in the $a\ ^3B_2$ state of the NO_2^+ parent. This state was observed to be branching predominantly into $NO^+ + O$ with a predissociation lifetime of about 300 ns. The cutoff photoelectron near 0.8 eV leaves the NO_2^+ parent at an energy around 13.13 eV which is around the energy of the (200) level in the $a\ ^3B_2$ state. This level was estimated to have a lifetime of 3.5 μs and this is long on the time scale of our ion acceleration. We will not detect this photoelectron in coincidence with a NO^+ fragment in our machine. We observe that for region (3) the kinetic energy of the $NO^+ + O$ fragments is much broader ranging from 0 eV up to the energetic boundary limit of about 0.9 eV. This broad distribution seems to reflect a much more statistical energy distribution from a predissociative mechanism in agreement with the observed lifetimes and fragmentation channels as reported by Eland and co-workers.[17,18] We do not observe any photoelectrons in coincidence with NO^+ frag-

ments with energies larger than 0.8 eV as such a prompt ejection of an electron after $(3+1')$ excitation leaves the NO_2^+ ion in the $a\ ^3B_2$ state at a low internal energy and a very long lifetime. Our coincidence imaging setup will not detect NO^+ fragment ions from NO_2^+ parent ions when they dissociate at very long time scales of tens to hundreds of microseconds.

Peak (7) is a transient photoelectron near 1.9 eV. It is correlated (not shown in the correlation plot) to NO^+ ions with a maximum of kinetic energy of 1.2 eV, completely analogous to the electron peak labeled with (2). From energetic considerations, it is clear that a $(3+1')$ excitation at 13.93 eV is not sufficient for the formation of $NO^+ + e$(1.9 eV). The next higher excitation is $(2+2')$ at 15.48 eV. As discussed before in Sec. IV A, there is no long lived state after two-photon excitation of 400.4 nm. So we do not see this peak at long delay times. However, apparently there is a favorable NO_2 geometry configuration in a time window around some 200 fs that a further absorption with two photons of 266 nm is enhanced to eject a photoelectron of 1.9 eV leaving the NO_2^+ ion at an energy of 13.58 eV. This energy is exactly at the location of the fast dissociative $b\ ^3A_2$ (000) state, see Table I. Because the NO^+ is formed with kinetic energy of about 1.2 eV, we attribute the transient peak (7) from a $(2+2')$ process occurring only at a favorable geometry after some dynamics after absorption of one (or two) photons at 400.4 nm followed by prompt electron ejection and direct fast dissociation of NO_2^+ on the $b\ ^3A_2$ state.

So, in summary the predominant feature labeled (2) is from $(3+1')$ excitation to the fast direct dissociative $b\ ^3A_2$ state and feature (3) from a predissociative mechanism in the $a\ ^3B_2$ state. Feature (6) is from prompt ionization after a $(3+1')$ excitation leaving the NO_2^+ system at an energy just above threshold for fragmentation leading to very slow NO^+ fragments. Transient peak (7) is from $(2+2')$ absorption followed by prompt photoelectron ejection and fast direct dissociation on the $b\ ^3A_2$ state.

2. Long time delay

At long delay time there are only three electron peaks remaining in the correlated (e, NO^+) events. Photoelectrons of 0 eV, peak (1), and photoelectrons of about 0.9 eV, peak (4), and a transient peak (5) at 1.2 eV.

Figures 5, 7(b), and 7(c) show that the dominant electron peak at large positive pump-probe delay times (500 – 1750 fs) is the region of zero kinetic energy electrons [labeled with (1)], which is bounded by the available energy of nearly 0 eV for dissociation into $NO^+ + O$ after $(1+2')$ excitation. The correlation plot of Fig. 7(c) shows that these near zero kinetic energy electrons correlate with almost zero kinetic energy NO^+ ionic fragments. The fact that this electron peak is observed at a long delay time for the 266.9 nm probe laser leads to the conclusion that one 400.4 nm photon has to be absorbed leading to an excited state in the neutral NO_2 parent molecule which needs to be relatively long lived (picoseconds) to enable further excitation with the 266.9 nm probe pulse. Subsequently, two 266.9 nm (4.65 eV) photons will ionize the parent molecule, followed by dissociation to give NO^+ fragments with near 0 meV kinetic energy. This $(1+2')$ excitation at 12.39 eV followed by prompt ejection of a very slow photoelectron leaves the NO_2^+ ion just above the thermodynamic threshold for the formation of $NO^+(^1\Sigma) + O(^3P) + e$ of 12.38 eV. It is not likely to have a strong fast dissociation channel after one photon 400.4 nm (3.096 eV) absorption, because only less than 10% of the spectrum of the pump pulse lies above the dissociation threshold giving $NO(X\ ^2\Pi) + O(^3P)$ at $D_0 = 25\ 128.56\ cm^{-1}$ (3.116 eV).[36,38] At shorter wavelengths, however, formation of neutral ground state NO was previously observed by Singhal *et al.*[24] after excitation with a wavelength at 375.3 nm. Therefore, we assign peak (1) to absorption of one photon of 400.4 nm to the long lived vibronically coupled $X, A\ ^2B_2$ system, followed by two-photon absorption of 266.9 nm and slow statistical dissociation of NO_2^+.

The electron peak labeled (4) with an electron energy of 0.9 eV is only observed when the 400.4 nm laser acts as the pump laser. López-Martens *et al.*[25] reported the formation of free neutral electronically excited $NO(A\ ^2\Sigma)$ after absorption of three 400 nm photons. On the contrary, Form *et al.*[8] did not observe an electron peak near 0.9 eV. Indeed the absorption of one 266.9 nm photon by a free neutral $NO(A\ ^2\Sigma)$ fragment leads to a 0.9 eV photoelectron. Additionally, the NO^+ signal clearly persists at long delay time between the 400.4 nm pump pulse and the 266.9 nm probe pulse. These were mentioned as two necessary conditions by Form *et al.*[8] for $NO(A\ ^2\Sigma)$ production. So our results here, and also the photoelectron spectrum observed in our other experiment, reported elsewhere using noncoincident photoelectron and photoion imaging,[28] clearly show a 0.9 eV electron peak in support of the measurements of López-Martens *et al.*[25] and the mechanism of a $(3+1')$ process.

The maximum kinetic energy expected for the $NO^+(v=0) + O(^3P)$ channel, created by this $(3+1')$ photon pathway, is 0.7 eV and the correlation plot in Fig. 7(c) shows that the total kinetic energy of peak (4) is limited to 0.4 eV. This must mean that the ionization takes place toward $NO^+(v=1)$ in the first vibrational excited state, which accounts for the 0.3 eV of energy. The free neutral $NO(A)$ in the first vibrational state is ionized by one 266.9 nm photon toward NO^+ in the first vibrational state. The appearance energy of this channel is located 0.3 eV higher in energy, i.e., at 12.68 eV. This has to be subtracted from the energy available in the $(3+1')$ photon process, which gives a line parallel to the $(3+1')$ line in Figs. 7(b) and 7(c). This line is located at lower energy and the maximum of available energy to be distributed over the kinetic energy of the ion and electron is now only 1.25 eV. López-Martens *et al.* observed $NO(A\ ^2\Sigma)$ production in the vibrational ground state, the first and probably also the second vibrationally excited state after absorption of three 400 nm photons. It is completely in agreement with our data, because the kinetic energy of the fragments is limited to 0.7 in the ground state, 0.4 eV in the first vibrational state. A small increase in anisotropy for these electrons is observed from $\beta_{2,\mathrm{lab},e}(4) = 0.9$ at short delay times to $\beta_{2,\mathrm{lab},e}(4) = 1.2$ at long delay times. We also see a transient electron peak at 1.2 eV for delay time of about 500 fs, peak (5) in Fig. 5. Apparently, there is some dynamics at the three-

photon level that produces an optimum window for photoionization and production of very slow $NO^+(v=1)$ leading to a photoelectron of 1.2 eV.

So, in summary the dominant feature labeled (1) is from $(1+2')$ excitation near the thermodynamic dissociation threshold leading to a slow statistical dissociation of NO_2^+. The features (4),(5) are from a $(3+1')$ process inducing the dissociation of a highly excited neutral state in NO_2 leading to electronically excited $NO(A\ ^2\Sigma\ v=1)+O(^3P)$ and followed by one-photon ionization of the neutral NO fragment. Transient peak (7) is from $(2+2')$ absorption followed by prompt photoelectron ejection and fast direct dissociation of NO_2^+ on the excited $b\ ^3A_2$ state.

3. Recoil-frame photoelectron angular distribution

In Fig. 8, three different photoelectron angular distributions are shown. The angular probability distribution for electron recoil at a particular angle with the recoil direction of the NO^+ fragment is plotted, the RFPAD. In panels A and B, we selected two different sets of (NO^+, e) events at zero delay time, panel A displays the RFPAD of events in region (3) with relatively slow NO^+ with kinetic energy of (0.3 ± 0.1) eV and electrons with energy of (0.65 ± 0.06) eV, and panel B displays the RFPAD of events in region (2) with relatively fast NO^+ kinetic energy of (1.0 ± 0.1) eV and electrons with energy of (0.35 ± 0.03) eV. As can be seen, the two RFPADs are quite different and we can further quantify the RFPAD by an expansion in Legendre polynomials, $I_{rf,e}=1+\Sigma\beta_{i,rf,e}P_i$, with $i=1-4$. We obtain $\beta_{1,rf,e}(A)=0.6$, $\beta_{2,rf,e}(A)=1.1$, $\beta_{3,rf,e}(A)=0.4$, $\beta_{4,rf,e}(A)=0.4$ for the distribution in panel A, and $\beta_{1,rf,e}(B)=0.13$, $\beta_{2,rf,e}(B)=0.84$, $\beta_{3,rf,e}(B)=0.16$, $\beta_{4,rf,e}(B)=-0.23$. Clearly, the distribution in panel A is much more anisotropic with a larger probability for ejecting the electron in a similar direction as the recoiling ion. The distribution in panel B appears also somewhat anisotropic with respect to the NO^+ recoil direction, but also wider with more intensity at directions perpendicular to the NO^+ recoil direction. As discussed above, we attribute the events in region (3) (panel A) to a $(3+1')$ excitation with a photoelectron leaving the NO_2^+ ion in the $a\ ^3B_2$ state, the events in region (2) (panel B) to the same $(3+1')$ process but ejecting an electron leaving the NO_2^+ ion in the $b\ ^3A_2$ state. The symmetries of these final electronic states are different. Of course, also the character of the excited (Rydberg) state after 3×400.4 nm photon excitation plays an important role in the angular distribution of the ejected electron. At this moment, we do not have any more semiquantitative information about the molecular orbitals involved and this awaits further theoretical studies.

Eland and co-workers[17,18] observed that the (NO^+, e) angular correlation in the recoil frame for this $b\ ^3A_2$ (000) state is opposite, i.e., the electron departs in the opposite direction to the NO^+ recoil direction. This was for one-photon ionization at high energies around 27 eV. Furthermore, it is interesting to note that in the synchrotron experiments by Toffoli *et al.*[26] after one photon excitation at 14.4 eV the electrons were preferentially ejected in the plane of the NO_2 molecule when the polarization of the radiation was perpendicular to the molecular plane. It is clear that in our multiphoton excitation at 13.93 eV the RFPAD is quite different reflecting the very different excitation process and molecular orbitals involved.

In panel C of Fig. 8, we selected (NO^+, e) events at 2000 fs delay time, resulting in the RFPAD of events in region (4) with relatively slow NO^+ with kinetic energy of (0.3 ± 0.1) eV and fast electrons with energy of (0.93 ± 0.05) eV. These events were attributed to the ionization of neutral $NO(A\ ^2\Sigma\ v=1)$ fragments by one-photon ionization with 266.9 nm. As can be seen the RFPAD is forward-backward symmetric (within experimental noise) which is to be expected for photoionization of a neutral diatomic fragment. The Legendre expansion only has a significant $\beta_{2,rf,e}(C)=1.3$, very similar to what has been observed in other photoionization experiments of $NO(A\ ^2\Sigma)$.[39,40]

More detailed insight of the exact excited states involved in the multiphoton ionization and fragmentation dynamics can be obtained by determining the molecular frame photoelectron angular distributions. We intend to discuss these RFPADs in more detail in a future publication.

V. CONCLUSION

In this paper, we present the first experimental results obtained with the newly constructed femtosecond time-resolved photoelectron-photoion coincidence imaging machine at the LCVU in Amsterdam. We have assigned various time-dependent multiphoton multichannel pathways in NO_2 resulting from a two color pump-probe excitation at 400 and 266 nm.

The photoionization dynamics leading to the formation of a stable NO_2^+ parent ion and photoelectrons up to 2 eV is dominated by $(1+2')$ and $(3+1')$ excitation processes. Transient changes of the photoelectron spectra are attributed to nonadiabatic dynamics between the ground state and the $A\ ^2B_2$ state after absorption of a 400 nm photon. Furthermore, Rydberg states in NO_2 are used as intermediate stepping states in the multiphoton excitation to enable ionization from the bent ground state of the neutral NO_2 to the linear ground state of NO_2^+ and the formation of rather narrow photoelectron peaks in coincidence with NO_2^+.

Both the statistical and fast direct dissociations of NO_2^+ photodynamics are attributed to the fragmentation into $NO^+ + O + e$ from $(1+2')$ and $[(3+1'), (2+2')]$ multiphoton excitation, respectively. Prompt ejection of various photoelectrons leaves the NO_2^+ ion in conformations on the ground state and the electronically excited $a\ ^3B_2$, $b\ ^3A_2$ states, which are energetically above the dissociation threshold. This results in fragmentation to $NO^+ + O$ with varying amounts of kinetic energy of the molecular fragments. At short pump probe delay times, the dominant photon pathway for NO^+ formation is a 3×400 nm$+1\times266$ nm multiphoton excitation. At long delay times (>500 fs) two different pathways are observed. The most dominant is the 1×400 nm$+2\times266$ nm photon pathway giving rise to very slow electrons and NO^+ ions. However, also, the absorption of 3×400 nm photons to excited NO_2 (Rydberg) states followed by dissociation toward neutral and electronically excited

$NO(A\,^2\Sigma, v)+O$ fragments is observed. The $NO(A\,^2\Sigma, v)$ fragment is predominantly formed in the vibrationally excited $v=1$ state, but a minor transient $NO(A, v=1)+O$ channel is also observed. Subsequent absorption of a single 266 nm photon by the neutral $NO(A\,^2\Sigma, v)$ fragment leads to ionization of NO^+.

The results presented here elucidate some of the complex multiphoton multichannel pathways observed in the photodynamics of a small molecule such as NO_2 using femtosecond pulses. Even more insight about the photoionization dynamics can be obtained from the recoil-frame (molecular frame) photoelectron angular distribution. Preliminary data are presented here for three different RF-PADs. The full analysis of these and other angular distributions is still in progress and is intended to be presented in the near future.

ACKNOWLEDGMENTS

This research has been financially supported by the council for Chemical Sciences of the Netherlands Organization for Scientific Research (NWO-CW VICI program). W.G.R. gratefully acknowledges the support of the European Union through a Marie Curie Outgoing International Fellowship under Contract No. OIF 021907. The authors would like to thank Dr. C. C. Hayden for many helpful discussions on coincidence imaging. W.G.R. would like to thank Dr. D. W. Chandler and Dr. C. C. Hayden for the opportunity to visit and work at the Combustion Research Facility of Sandia National Laboratories, Livermore. M.H.M.J. would like to thank Dr. G. Theodorakopoulos and Dr. R. Jost for helpful discussions on Rydberg states and nonadiabatic dynamics in NO_2.

[1] D. W. Chandler and P. L. Houston, J. Chem. Phys. **87**, 1445 (1987).
[2] A. T. J. B. Eppink and D. H. Parker, Rev. Sci. Instrum. **68**, 3477 (1997).
[3] M. N. R. Ashfold, N. H. Nahler, A. J. Orr-Ewing, O. P. J. Vieuxmaire, R. L. Toomes, T. N. Kitsopoulos, I. A. Garcia, D. A. Chestakov, S.-M. Wu, and D. H. Parker, Phys. Chem. Chem. Phys. **8**, 26 (2006).
[4] A. G. Suits, M. Kawasaki, and W. Lawrance, Phys. Chem. Chem. Phys. **8**, 2913 (2006).
[5] A. Delon and R. Jost, J. Chem. Phys. **95**, 5686 (1991).
[6] E. A. Volkers, J. Bulthuis, S. Stolte, R. Jost, N. Wehres, and H. Linnartz, J. Mol. Spectrosc. **245**, 1 (2007).
[7] A. T. J. B. Eppink, B. J. Whitaker, E. Gloaguen, B. Soep, A. M. Coroiu, and D. H. Parker, J. Chem. Phys. **121**, 7776 (2004).
[8] N. T. Form, B. J. Whitaker, L. Poisson, and B. Soep, Phys. Chem. Chem. Phys. **8**, 2925 (2006).
[9] M. Sanrey and M. Joyeux, J. Chem. Phys. **126**, 074301 (2007).
[10] Y. Arasaki and K. Takatsuka, Chem. Phys. **338**, 175 (2007).
[11] W. G. Roeterdink and M. H. M. Janssen, Phys. Chem. Chem. Phys. **4**, 601 (2002).
[12] L. Wang, H. Kohguchi, and T. Suzuki, Faraday Discuss. **113**, 37 (1999).
[13] R. E. Continetti and C. C. Hayden, Coincidence imaging techniques, in *Modern Trends in Reaction Dynamics*, edited by X. Yang and K. Liu (World Scientific, Singapore, 2004), pp 475–528.
[14] R. S. Tapper, R. L. Whetten, G. S. Ezra, and E. R. Grant, J. Phys. Chem. **88**, 1273 (1984).
[15] H. Matsui, J. M. Behm, and E. R. Grant, J. Phys. Chem. A **101**, 6717 (1997).
[16] P. Bell, F. Aguirre, E. R. Grant, and S. T. Pratt, J. Phys. Chem. A **108**, 9645 (2004).
[17] P. Baltzer, L. Karlsson, B. Wannberg, D. M. P. Holland, M. A. MacDonald, M. A. Hayes, and J. H. D. Eland, Chem. Phys. **237**, 451 (1998).
[18] J. H. D. Eland and L. Karlsson, Chem. Phys. **237**, 139 (1998).
[19] G. Jarvis, Y. Song, C. Ng, and E. Grant, J. Chem. Phys. **111**, 9568 (1999).
[20] J. A. Davies, J. E. LeClaire, R. E. Continetti, and C. C. Hayden, J. Chem. Phys. **111**, 1 (1999).
[21] J. A. Davies, R. E. Continetti, D. W. Chandler, and C. C. Hayden, Phys. Rev. Lett. **84**, 5983 (2000).
[22] A. M. Rijs, M. H. M. Janssen, E. T. H. Chrysostom, and C. C. Hayden, Phys. Rev. Lett. **92**, 123002 (2004).
[23] O. Gessner, A. M. D. Lee, J. P. Shaffer, H. Reisler, S. V. Levchenko, A. I. Krylov, J. G. Underwood, H. Shi, A. L. L. East, D. M. Wardlaw, E. t. H. Chrysostom, C. C. Hayden, and A. Stolow, Science **311**, 219 (2006).
[24] R. P. Singhal, H. S. Kilic, K. W. D. Ledingham, C. Kosmidis, T. McCanny, A. J. Langley, and W. Shaikh, Chem. Phys. Lett. **253**, 81 (1996).
[25] R. B. López-Martens, T. W. Schmidt, and G. Roberts, J. Chem. Phys. **111**, 7183 (1999).
[26] D. Toffoli, R. R. Lucchese, M. Lebech, J. C. Houver, and D. Dowek, J. Chem. Phys. **126**, 054307 (2007).
[27] A. Vredenborg, W. G. Roeterdink, and M. H. M. Janssen, Rev. Sci. Instrum. (in print) (2008).
[28] D. Irimia and M. H. M. Janssen (unpublished).
[29] T. Luhmann, Rev. Sci. Instrum. **68**, 2347 (1997).
[30] G. P. Bryant, Y. Jiang, M. Martin, and E. R. Grant, J. Chem. Phys. **101**, 7199 (1994).
[31] K. S. Haber, J. W. Zwanziger, F. X. Campos, R. T. Wiedmann, and E. R. Grant, Chem. Phys. Lett. **144**, 58 (1988).
[32] D. E. Clemmer and P. B. Armentrout, J. Chem. Phys. **97**, 2451 (1992).
[33] N. Shafer, K. Tonokura, Y. Matsumi, S. Tasaki, and M. Kawasaki, J. Chem. Phys. **95**, 6218 (1991).
[34] J. Lievin, A. Delon, and R. Jost, J. Chem. Phys. **108**, 8931 (1998).
[35] I. D. Petsalakis, G. Theodorakopoulos, and M. S. Child, J. Chem. Phys. **115**, 10394 (2001).
[36] R. Jost, J. Nygard, A. Pasinski, and A. Delon, J. Chem. Phys. **105**, 1287 (1996).
[37] webbook.nist.gov.
[38] S. J. Matthews, S. Willitsch, and T. P. Softley, Phys. Chem. Chem. Phys. **9**, 5656 (2007).
[39] J. R. Appling, M. G. White, W. J. Kessler, R. Fernandez, and E. D. Poliakoff, J. Chem. Phys. **88**, 2300 (1988).
[40] S. W. Allendorf, D. J. Leahy, D. C. Jacobs, and R. N. Zare, J. Chem. Phys. **91**, 2216 (1989).